Preflight Summary Report for: SNS-AI manuscript-edited v2.pdf

Profile: Convert to PDF/A-1b (Processed pages 1 to 28)

Processed by Sophia S, Date: 12/14/20 4:01 PM

Fixups

- Prepare annotations for PDF/A-1 (2 objects)
- Convert to PDF/A-1b (2 objects)
- Force blend color space to sRGB (13 objects)
- Make document XMP Metadata compliant with PDF/A-1 (1 object)
- Flatten transparency (high resolution, no decalibration of ICCbased CMYK) (1 object)
- Remove document structure compression (1 object)
- Compress all uncompressed objects using lossless ZIP compression (1 object)
- Recompress LZW as ZIP (1 object)
- Adjust colors for PDF based ISO standards (1 object)
- Fix font encoding (CIDSet) (11 objects)
- Fix font encoding (CIDToGIDMap) (5 objects)
- Convert SMask to image mask (12 objects)
- Insert missing Type entry in StructElem objects (857 objects)
- Remove unnecessary transparency groups (12 objects)

Results (Summary)

✔ **No problems found**

Document information

File name: "SNS-AI manuscript-edited v2.pdf"
Path: "/Users/sophias/Desktop"
PDF version number: "1.4"
File size (KB): 1021.5
Author: "Sophia s"
Creator: "Acrobat PDFMaker 20 for Word"
Producer: "Adobe PDF Library 20.13.106"
Created: "12/14/20 8:49 PM"
Modified: "12/14/20 4:00 PM"
Trapping: "Unknown"
Number of plates: 4
Names of plates: "(Cyan) (Magenta) (Yellow) (Black) "

Environment

Preflight, 18.4.0 (249)
Acrobat version: 20.013
Operating system: macOS 10.16.0

Aluminum ions speciation and transport in acidic deep eutectic $AlCl_3$ amide electrolytes

Domenec Paterno,[1] Emma Rock,[1] Andrew Forbes,[1] Rija Iqbal,[1] Nomon Mohammad,[2] Sophia Suarez[1,3]

[1]Department of Physics, Brooklyn College of CUNY, Brooklyn, NY 11210
[2]Biology Department, Hunter college of CUNY, New York, NY 10065
[3]Physics Department, The Graduate Center of CUNY, New York, NY 10016

Abstract: Aluminum ion speciation in $AlCl_3$:amide deep eutectic solvents (DES) were explored using variable temperature multi-Nuclear (^1H and ^{27}Al) Magnetic Resonance and Electrochemical Impedance Spectroscopies. Focus was on the interplay between the local and bulk interactions on species transport, and the effect of $AlCl_3$ concentration on their dynamics. Acetamide, butyramide and propionamide were chosen and molar ratios of 1:1 – 1.7:1 of $AlCl_3$:amide were studied. Calculated Walden products show that although the DES electrolytes are 'subionic,' they are more conductive than 'poor ILs'. The ionic conductivity data showed VFT temperature dependences, and calculated fragility values were less than 5 for all three amides and concentrations, indicating high levels of conformational mobility for the aluminum species. ^1H chemical shift data showed increased shielding with increasing molar ratios for all three amides indicating an enhancement in the local electron densities, possibly due to an increase in the more shielded *cis* conformation population. ^{27}Al spectra revealed multiple aluminum species that experienced both intermediate and fast chemical exchanges with increasing $AlCl_3$ concentration. The $AlCl_2(amide)_2^+$ species population decreased with both increasing temperature and $AlCl_3$ concentration, especially for shorter alkyl chains amides. This suggests it plays a less significant role in the aluminum ion transport at higher $AlCl_3$ concentration. ^{27}Al T_1 values for the various species revealed a temperature and concentration dependent plateauing in the T_1 of the $AlCl_2(amide)^+$ species for molar ratios greater than 1:1. Additionally, with increasing $AlCl_3$ concentration, the merging of the $AlCl_4^-$ and $[AlCl_2(amide)_2]^+$ species resulted in its T_1 being the shortest and increasing with increasing temperatures, suggesting it experiences greater electric field gradients compared to the other aluminum species.

Keywords: NMR, spin-lattice relaxation, ionic conductivity, VFT, aluminum species.

Introduction:

The world's energy needs require the availability of cheap, reliable, efficient and safe electrochemical energy storage (EES) devices. This is especially necessary as the world focuses more on renewable and environmentally friendly but unfortunately intermittent sources such as wind and solar. EES devices such as batteries, fuel cells, and supercapacitors have been developed and are in some cases commercialized. Of the current EES technologies, batteries – especially lithium ion types – have been most successful [1-4]. Lithium ion batteries (LIBs) serve as the benchmark for EES devices especially for low temperature portable and automotive applications because they deliver about 2.5 times the energy compared to others (lead-acid, nickel-metal hydride, nickel-cadmium)[3]. This is due to several factors including lithium's low molecular weight, and the efficiency and longer cycle life of the batteries [3]. Despite these advantages, issues such as cost, safety and lithium reserves location exist that make finding alternatives

necessary [4-9]. Together, these provide the need for implementation of more wide-scale competitive alternative EES devices.

One niche alternative EES device is the aluminum (Al) ion battery (AIB). This is because of aluminum metal's three-electron redox property, favorable energy density (theoretical 2980 mAh/gm compared to lithium's 3860 mAh/gm), its status as the earth's most abundant metal element, its low reactivity, ease of handling, high cyclability and low cost. For example, the Al-air battery which is comprised of an Al anode, air cathode and suitable electrolyte, with a theoretical voltage of 2.7 V and energy density of 8.1 kWh/kg, is being considered for future large-scale applications. Unfortunately, Al has a high open-circuit potential (-1.66 V vs. a standard Hg/HgO with a 4M NaOH electrolyte at 25ºC) [10], which prevents the use of highly conducting aqueous electrolytes due to the decomposition of water before deposition of Al. Additionally, Al has a strong affinity towards oxygen and hence cannot be electrolyzed from aqueous solutions [11]. Most detrimental is the formation of protective oxide layers on the surface of Al which although provides excellent corrosion resistance, prevents the use of Al as an anode material. In order to take advantage of the stated advantages of Al and further development and optimization of the Al-air battery, optimized non-aqueous electrolytes are therefore needed.

Recently, deep eutectic solvents (DES) [12-19] have gained attention as electrolytes for EES devices [13-16]. These solvents are best defined as mixtures of ionic and non-ionic solid compounds with melting points much lower than the pure compounds. Their thermal and physical properties are similar to room temperature ionic liquids, but they are generally cheaper and easier to prepare. In the case of metal halides, the eutectic formation rests with their asymmetric splitting whereby anions and donor-coordinated cations are formed [12]. In the case of the $AlCl_3$, this process results in the formation of anionic and cationic structures such as $AlCl_4^-$, $Al_2Cl_7^-$, and $[AlCl_2(amide)_n]^+$ where n = 1 and 2 [12], depending on the $AlCl_3$:amide molar ratio. With regards to reversible electrodepositing of Al metal, $AlCl_3$:amide molar ratios greater than 1.0 are needed [13]. Like ionic liquids, the transport properties of DESs can be tuned, but because of the abundance of tuning options, fundamental studies of the eutectic components and their combinations are needed.

In our efforts to advance the development of AIBs, we investigated the fundamental ion dynamics in varying concentrations of $AlCl_3$:amide mixtures using variable temperature multi-Nuclear (^1H, ^{27}Al) Magnetic Resonance (NMR) and Electrochemical Impedance (EIS) spectroscopies. Our goal was to determine how the aluminum ion transport and speciation were affected by the amide type, relative concentration and temperature. The amides investigated were acetamide, butyramide, and propionamide. These were chosen because they differ in the alkyl chain length which may help in elucidating the electron donor capabilities of the amides and the resulting aluminum ion species formed. Additionally, some NMR [16-17,19] spectra – which will be discussed below, and bulk properties (ionic conductivity, viscosity and density) [21] data [12, 21] already existed. To characterize the ion dynamics, NMR spin-lattice relaxation time (T_1), chemical shifts and lineshapes were determined.

In the study of ion and mass transports in electrolytes, NMR is one of the most applied and trusted tools because it offers a direct and non-destructive probe of the nuclei local environment, and is capable of providing information on dynamics over a wide time ($1 – 10^{-10}$ sec) scale [22-30]. In the study of acidic $AlCl_3$:[EMIM]Cl - the most common aluminum ion electrolyte - high resolution ^{27}Al NMR spectra [16, 30-32] revealed the presence of two distinct peaks, which have been attributed to the presence of the anionic $AlCl_4^-$ and $Al_2Cl_7^-$ species. It should be noted however that the $Al_2Cl_7^-$ assignment bears some controversy in that its chemical shift and

appearance seem to be dependent on the mixture's moisture composition [28-29]. It should also be noted that these studies focused mainly on lineshapes and most were done at room temperature. In the case of DES, Abood et.al. [18] studied the $AlCl_3$:acetamide using ^{27}Al NMR lineshape and assigned the three main peaks at ~101, 89 and 74 ppm for the 1:1 molar ratio electrolyte to the presence of $AlCl_2(amide)_2^+$, $AlCl_4^-$, and $AlCl_2(amide)^+$ species respectively. Angell et. al. [17] studied the 1.3:1 molar ratio $AlCl_3$:urea electrolyte using both Raman and ^{27}Al NMR lineshapes and found similar peaks. They surmised that Al metal had two deposition routes, namely through the $Al_2Cl_7^-$ anions and the $AlCl_2(urea)_n^+$ cations. In another example, Coleman et.al. [19] performed ^{27}Al NMR on the $AlCl_3$:acetamide system and observed the presence of three main ionic species at ~101, ~89 and ~74 ppm, and assigned them as $AlCl_4^-$, $[AlCl_3(amide)]$, and $[AlCl_2(amide)_2]^+$ respectively. Hu et.al. [16] determined the steric effect of methyl groups on the $AlCl_3$:amide DES for acetamide, N-methylacetamide, and N,N-dimethylacetamide using various techniques, including room temperature ^{27}Al NMR lineshapes. They – like Coleman - assigned the three observed aluminum peaks at ~103, 89 and 77 ppm to the $AlCl_4^-$, $AlCl_3L_n$ and $AlCl_2L_n^+$ species respectively and they also surmised that the greater the symmetry of the methyl groups, the greater the concentration of $AlCl_4^-/Al_2Cl_7^-$ formation. It should be noted that these assignments are also not without controversy as: (1) they assume complete solvation of the $AlCl_3$ compound, and (2) were done by mass spectrometry, which has been shown to give incorrect species identification in the case of chlorometallate anions [20]. Assignments of neutral species have also been done which implies incomplete solvation [20]. In spite of the deviations on peak assignments', a noted lack in these studies is dynamical information, especially as a function of temperature. Because these materials are being considered for applications where their dynamical attributes are most needed, it is clear that better insight into aluminum ion speciation and more importantly – their dynamics - are needed. It should be noted that although the $AlCl_3$:amide DESs being studied contains several NMR active nuclei (^1H, ^{13}C, ^{15}N, ^{17}O, and ^{27}Al), most studies have focused almost exclusively on ^{27}Al. This may be due to the fact that nitrogen, carbon and oxygen all have extremely low natural abundance and sensitivity compared to aluminum, both of which makes NMR studies difficult even under normal circumstances. The smaller number of ^1H studies on these mixtures also supports the aluminum as being the most important atom, almost to the exclusion of all else. While this may be the case, as the results show the ^1H perspective could also be valuable in deciphering the dynamics and various ionic interactions.

Experimental:

Sample Preparation: The electrolytes studied were varying concentrations of the amides: acetamide (**AA**, **AcA**, CH_3CONH_2, Alfa Aesar, > 99%), butyramide (**BA**, **BuA**, $CH_3CH_2CH_2CONH_2$, Frontier Scientific, > 99%), and propionamide (**PA**, **PrA**, $CH_3CH_2CONH_2$, Frontier Scientific, 99%), with Aluminum chloride ($AlCl_3$, Alfa Aesar, > 99%). Chemical structures of these amides are shown in Figure 1. The amides were dried in a vacuum oven at 353K for 40 hours while the $AlCl_3$ was used as received. Both $AlCl_3$ and the amides were combined in their appropriate masses to create the required molar ratios of mixtures, which were mixed slowly with a magnetic stirrer to form the resulting liquid. The work was done in a glove box under constant flowing nitrogen atmosphere. The exothermic nature of the reaction eliminated the need for heating or vigorous mixing.

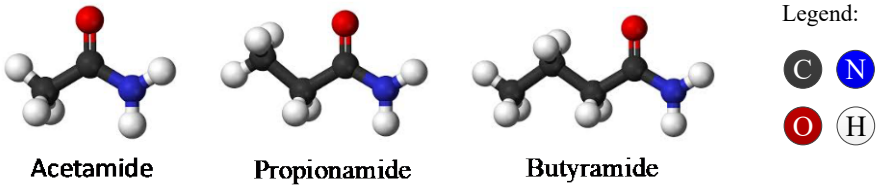

Figure 1. Chemical structures for the amides.

NMR: ^{1}H and ^{27}Al spectra and spin-lattice relaxation times (T_1) were determined at 300 and 78 MHz respectively on a Varian Unity Plus spectrometer over the temperature range of 293-363K for all mixtures. Increment of 10°C and temperature equilibration times of 15-20 minutes were used for all measurements. A Nalorac z-spec 5mm BB probe was used to determine ^{1}H and ^{27}Al spectra and T_1 data. All samples were packed into 5mm glass tubes under constant flowing nitrogen atmosphere and sealed with Teflon caps. All measurements were repeated four times and the results presented are the average of all. Spin-lattice relaxation measurements were conducted using an inversion recovery pulse sequence $\left(\pi - \tau - {}^{\pi}/_{2} - Acq\right)$ for an array of 20 values for the delay, τ. The resulting data were fit to Equation 1 [21-22]:

$$I(\tau) = I_0\left(1 - 2e^{-\tau/T_1}\right) \qquad [1]$$

Here, I represents the integral of the NMR signal, τ is the delay used between pulses, and T_1 is the characteristic spin-lattice relaxation time. A minimum of 5 T_1s were used as a delay between repetitions and uncertainties were ~5% for each value of T_1.

EIS Ionic Conductivity: Ionic liquid samples were packed in a dry nitrogen atmosphere into an airtight 3 mL (Biologic Brand) two-electrode sample cell, leaving 50% of the cell volume available for thermal expansion. The cells were temperature controlled from 288 to 363K using a silicone oil bath. The electrochemical impedance measurements were done using a Solartron 1260 Impedance Analyzer coupled with a Solartron 1287 Electrochemical Interface. Experimental parameters utilized a frequency sweep from 25 Hz to 2.5 MHz using a resolution of 20 data points per decade and the energization was set with AC amplitude of 10 mV with no DC offset. The resulting Nyquist plot of reactance versus resistance was inspected to determine the real electrical resistance. Using the corresponding cell constants and the electrical resistance, conductivity was calculated and plotted versus temperature. Data shown and discussed are the averages of three sets of measurements.

Background:
For spin $\boldsymbol{I}$ = 1/2 systems, generally the most dominant relaxation mechanism is the dipole-dipole (DD). This refers to the magnetic coupling between neighboring spins, and for spins I_i and I_k the interaction can be represented by the Hamiltonian H_D as [21-22]:

$$H_D = \sum_{j<k} b_{jk}\left(3\left(\boldsymbol{I_j}\cdot\boldsymbol{e_{jk}}\right)\left(\boldsymbol{I_k}\cdot\boldsymbol{e_{jk}}\right) - \boldsymbol{I_j}\cdot\boldsymbol{I_k}\right) \qquad [2]$$

where $\boldsymbol{e_{jk}}$ is a unit vector parallel to the line joining the centers of the two nuclei, b_{jk} is the dipole-dipole coupling constant and is given by: $-\frac{\mu_o \gamma_j \gamma_k}{4\pi r_{jk}^3}\hbar$, γ_i and γ_k are the gyromagnetic ratios of the

two spins, $\hbar$ is the reduced Plank's constant and r_{jk} is the distance between the two spins. H_D consists of homonuclear and heteronuclear interactions and for protons in a diamagnetic (no unpaired electrons) spin system, the homonuclear term is often the largest. In the case of homonuclear DD interactions, the spin-lattice relaxation time T_1 can be represented by the Bloemburgen, Purcell, and Pound (BPP) relationship [22] given in Eq. 3:

$$\frac{1}{T_1} = C\left[\frac{\tau_c}{1+\omega_0^2\tau_c^2} + \frac{4\tau_c}{1+4\omega_0^2\tau_c^2}\right] \quad [3]$$

$$C = \frac{3}{10}\gamma^2\hbar^2\sum_j \frac{1}{r_j^6} \quad [4]$$

where τ_c and ω_0 represent the motional correlation time and observation frequency in rad/s, respectively. The r_j^{-6} term guarantees that mainly nearest neighbors dominate the relaxation process, especially for protons [22].
^{27}Al is a spin $\boldsymbol{I}$ = 5/2 nucleus, which means in addition to its magnetic moment it also has a quadrupole moment that allows it to interact with electric field gradients produced by the stochastic fluctuations in the asymmetric electron density at the site of the nucleus, and the charge distribution external to the nucleus [22]. The interaction is described by the Hamiltonian as [22]:

$$H_Q = \frac{eQ}{6I(2I-1)}\sum eq_{ij}\left[\frac{3}{2}\left(I_iI_j + I_jI_i\right) - \delta_{ij}I(I+1)\right] \quad [5]$$

Here eq_{ii} are the principal values of the electric field gradient at the nucleus, eQ is the quadrupole moment of the nucleus, and $I_{i,j}$ are the nuclear spins. When present, the quadrupole interaction is generally stronger than others and will therefore provide the most efficient relaxation mechanism.

Results and Discussion:

1. Conductivity Data:

Variable temperature ionic conductivity (σ) data were determined for all DES electrolytes and representative plots are shown in Figures S1-S3 of the Supporting Information for varying molar ratios of all analogues. The general behavior of σ was a dependence on amide type, molar concentration and temperature. Several factors can contribute to σ but mostly the biggest contributors are temperature, solution viscosity and the number of available charge carriers. We see the relationships between these parameters through the Nernst-Einstein (NE, left) and Stokes-Einstein (SE, right) equations (Eq. 6):

$$\sigma = \frac{Dq^2c}{k_BT} \quad \text{and} \quad D = \frac{k_BT}{4\pi r\eta} \quad [6]$$

where η, D, q, k_B, c, T and r are the solution viscosity, self-diffusion coefficient, charge of the carrier, Boltzmann constant, charge carrier concentration, temperature in Kelvin, and hydrodynamic radius respectively. It should be understood that both equations were developed for application to very dilute solutions and that in these solutions the ions are depicted as hard non-interacting spheres, moving through a continuum of viscosity η. Additionally, the ions are expected to be single entities. Because of these, large errors are often obtained from the application

of either equation to concentrated systems. The main sources of errors are usually due to concentration, relaxation or drag, and electrophoretic effects.

The concentration effect comes from the increase in probability for ion association due to inter-ionic effects caused by greater electrostatic interactions with increase in concentration. The result of this may be the formation of neutral ion pairs and larger aggregates, effectively reducing their involvement in the transport process. The relaxation effect arises from the dissolution of symmetry of the ionic atmosphere (solvation sphere) about the central ion in an electric field. Since positive and negative charges move in opposite directions in an electric field, the ionic atmosphere will be pulled away from the central ion, thus creating an asymmetric environment. This in turn 'drags' the central ion and reduces its mobility. The electrophoretic effect refers to the movement of solvent molecules with the ions in the electric field. Again, because anions and cations move in opposite directions under an externally applied electric field, this results in every ion being subjected to the friction from moving against such a flow. All these can reduce the ionic conductivity.

Several features were revealed by the conductivity data. Firstly, the conductivity for all concentrations and amide analogues increased with increasing temperature. This effect of temperature on the ionic conductivity is expected and is due to the increasing thermal energies, which translates to faster dynamics and reduced electrostatic interactions. Secondly, there was a maximum in σ for all three amide analogues. Figure 2 shows the 313K and 353K variable molar ratio isotherms for all three amides and their respective maxima. As shown, for both the propionamide and butyramide DES electrolytes a prominent maximum is visible at the 1.3:1 molar ratio. However, for the acetamide DESs a broad plateau starting at the 1.1:1 molar ratio at lower temperatures gave way to a more pronounced maximum at the 1.3:1 molar ratio at higher temperatures. Liu et. al. [21] also observed similar maxima for the three amides. This maximum may be due to a combination of factors. With increasing molar ratio, the ionic species increase, which in turn can increase the conductivity as shown in the NE equation. The effect of the viscosity is also a factor, which - as detailed by Liu [21] - decreased linearly with increasing molar ratio for the acetamide electrolytes, but exhibited a broad minimum between 1.1:1 and 1.3:1 molar ratios for both the propionamide and butyramide DES electrolytes. The minimum in η coincides well with the maximum in σ for both the propionamide and butyramide DES electrolytes and the decrease that follows may be the due to the increasing viscosity. In the case of acetamide, since its viscosity decreases with increasing molar ratio according to Liu et.al. [21], the decrease that follows its maximum may be attributed to the increasing $AlCl_3$ concentration and the shortness of its alkyl chain - compared to butyramide and propionamide – both of which limits the aluminum species mobilities due to increasing electrostatic interactions.

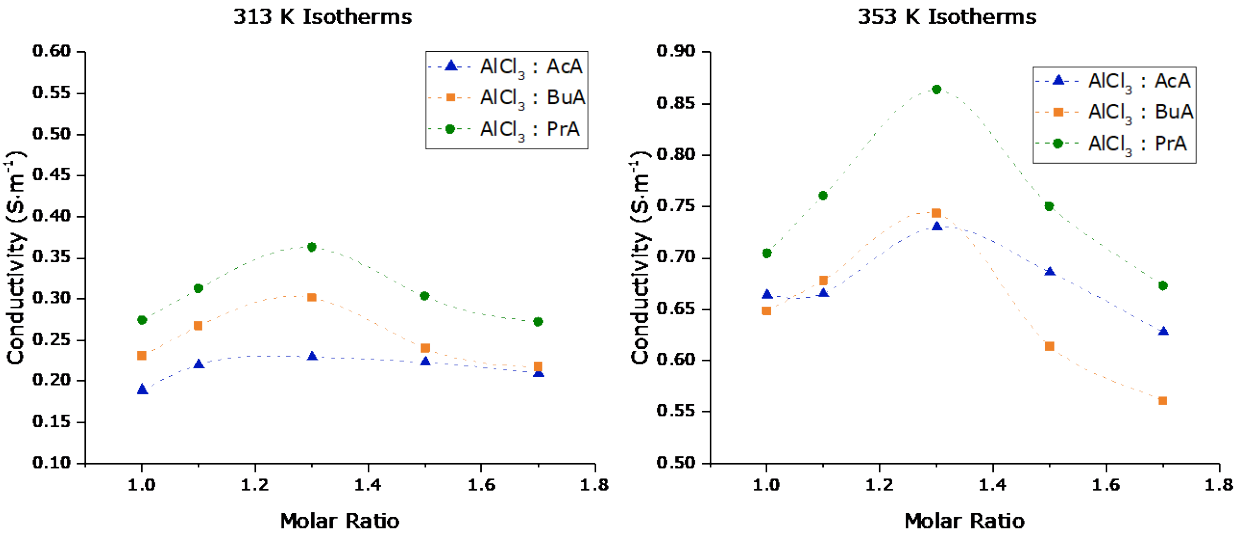

Figure 2. Ionic conductivity vs. molar ratio isotherms for $AlCl_3$:amide at 313K and 353K.

Thirdly, for all molar ratios the conductivity followed the general order of: PA > BA ≥ AA. From the NE and SE relationships, at a constant temperature and concentration, an increase in σ is associated with an increase in the self-diffusion coefficient, ergo a reduction in η. At the time of writing no self-diffusion coefficient data were available for the systems studied. Finally, as shown in Figure 3, the temperature dependence of the conductivity data can be fitted using the Vogel-Fulcher-Tamman (VFT) equation:

$$\sigma = \sigma_o \exp\left(\frac{-B}{T - T_o}\right) \qquad [7]$$

where the adjustable parameters - B, T and T_o - are the pseudoactivation energy, current temperature, and 'pseudo' ideal glass transition temperature respectively in unit of Kelvin. The logarithmic form of the VFT was used instead of the exponential as it allows better fitting of data spanning orders of magnitude. Additionally, when compared to the Arrhenius fit, the VFT produced smaller errors and had R^2 values greater than 0.99 indicating the VFT was a more suitable model. Generally, liquids obeying the VFT equation are described as 'fragile' [33], where dynamics are the result of available free volume and disorder resulting from molecular fluctuations and reorganizations over a wide variety of different particle orientations and coordination states, almost independently of thermal aid. The 'free volume' being referred to is the volume of unoccupied space in the mixture that allows diffusion processes [34-39]. Additionally, the more fragile a liquid, the greater its viscosity will decrease with increasing temperatures above its glass transition. The corresponding adjustable parameters and the correlation coefficient of determination (R^2) are given in Table 1. As shown, unlike the conductivity data for the $AlCl_3$:[EMIM]Cl system as reported by Ferrara et. al. [40], there was no monotonic decrease in the T_o value with increasing $AlCl_3$ concentration for any of the amides. Similarly, the pseudo activation energy did not display a monotonic increase with increasing $AlCl_3$ concentration. These indicate a significant difference between the ionic environments of the $AlCl_3$ DES analogues compared to the ionic liquid systems.

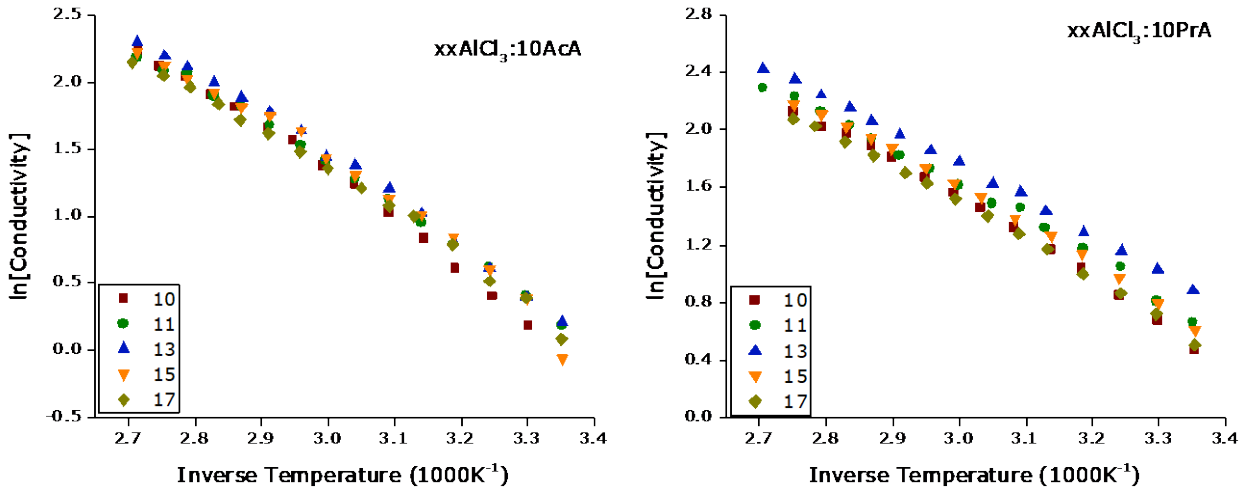

Figure 3. VFT plots of the ionic conductivity for $AlCl_3$:AA (left) and $AlCl_3$:PA (right) DES electrolytes.

There are also differences between the local environments of the amides as revealed by the conductivity results. The size of the amide molecules is as follows: BA>PA>AA and as previously stated, the PA analogues generally had the largest conductivity values while values for BA were slightly higher compared to AA at lower temperature, but either merged or were lower at higher temperatures. This suggests that amide size is a determining factor as it affects the resulting electrostatic interactions between the ionic species, as well as their mobilities. Whereas the acetamide appears too small to provide effective screening for the aluminum species especially at lower temperatures, the butyramide appears too bulky to provide efficient translational dynamics at higher temperatures. The propionamide however appears to balance effectively the need for effective electrostatic screening and translational dynamics.

To further investigate the screening afforded by the amides, we determined their Walden Product [41-44]. The Walden Product (Eq. 8) relates the molar ionic conductivity (Λ) and solution viscosity (η) through a temperature-dependent constant (k). It is a law often used to assess the ionic transport in ionic liquids and represents the degree of dissociation or iconicity according to the resulting classification of the liquid.

$$\Lambda\eta = k \qquad [8]$$

The reference used in the Walden Product is the very dilute 0.01M KCl solution, where the ions are considered to be completely dissociated and having equal mobilities. According to Angell et.al. [42, 44] 'good ionic liquids' are those for which their product is near the ideal line. Liquids with products above the ideal line are considered as 'superionic' while those below are considered 'subionic,' or 'poor ionic liquids.'

To determine the Walden products, we used the viscosity data determined by Liu et.al. [21]. Additionally, the molar ionic conductivity – which is determined by the dividing the determined conductivity by its molar concentration (density divided by molecular weight) – were determined using the density data of Liu et.al. [21]. Representative plots of the results are shown

in Figure 4 for the butyramide and propionamide analogues with concentrations from 1:1 – 1.7:1, and the corresponding values given in Table 2. The Walden product plots for acetamide are provided in Figure S4 of the Supporting Information. No density and viscosity data were available for the 1.7:1 molar ratio acetamide DES so its Walden product was not determined.

As shown, all the plots lie below the ideal line of the Walden product, regardless of temperature, amide type and molar concentration. Based upon the classifications given, the DESs are 'subionic'. However, upon further inspection they are above Angell's et.al. [42, 44] 'poor ILs' classification region. Typically, 'poor ILs' are those for which either cation-anion pairing is significant, or their respective motions are correlated. As will be discussed shortly, the aluminum species are chemically separated. Although the DESs are not completely 'poor ILs', they do have lower than expected ionic conductivities, which means there is some coordination between the cation and anion mobilities. In spite of this, additional support of their relatively good ion dynamics is provided by the fragility (D) values, which as shown in Table 1 are very small. Generally, fragility values for most ILs fall between 5 and 10. Those with values below 5 are considered 'most fragile.' This was demonstrated by Castner et.al. [45] in their study of the effect of the symmetry of fluorinated anions on dynamics in imidazolium based ILs. They obtained a value of 3.80 for the 1-ethyl-3-methylimidazolium bis(trifluoromethylsulfonyl)imide IL and attributed this to the effective inter-conversion between the *trans* and *cis* conformations of the anion that facilitated faster ion dynamics. Since the DES analogues contain anionic ($AlCl_4^-$, $Al_2Cl_7^-$), cationic ($[AlCl_2(amide)_n]^+$) and neutral ($[AlCl_3(amide)]$ and $[AlCl_3(amide)_2]$) aluminum species, the small fragility factors support the existence of local conformational changes of the various species. With regards to conformation, Olah et.al. [46] used DFT to determine the minimum energy configurations of the intermediate $AlCl_2^+$ species with various carbonyl and alkene compounds. They found in the case of formaldehyde ($H_2C{=}O$) and acetaldehyde (H_3C-$CH{=}O$), Al-O coordinated structures which offered greater conformational freedom for both the $AlCl_2^+$ and carbonyl compound. In the case of ethene ($H_2C{=}CH_2$) and propene ($H_2C{=}H$-CH_3) however, the main bonding was through the Al-C interactions which in the case of propene resulted in unbridged conformationally more mobile structures, whereas for ethene, interactions occurred through both the Al-C and Cl-C bonds, resulting in symmetrically bridged structures with less conformational freedom.

Table 1. VFT fitted parameters for ionic conductivity, including the Fragility (*F*) values. Pseudo-activation energies (*B*) are given in Kelvin but can be represented in kJ/mol using the conversion factor 1kJ/mol = 120.31 K.

	T_0	B	σ_0	F	R^2
Sample	(K)	(K)			
10AlCl3:10AcA	191 ± 9	623 ± 8	310 ± 8	3.3 ± 0.2	0.99936
11AlCl3:10AcA	175 ± 11	681 ± 10	307 ± 10	3.9 ± 0.3	0.99901
13AlCl3:10AcA	182 ± 11	651 ± 10	331 ± 12	3.6 ± 0.3	0.99877
15AlCl3:10AcA	232 ± 9	277 ± 5	69 ± 2	1.2 ± 0.1	0.99580
17AlCl3:10AcA	194 ± 12	522 ± 9	168 ± 6	2.7 ± 0.2	0.99814

10AlCl3:10BuA	191	±	6	520	±	5	159	±	3	2.7	±	0.1	0.99934
11AlCl3:10BuA	185	±	7	506	±	6	139	±	3	2.7	±	0.1	0.99915
13AlCl3:10BuA	175	±	14	571	±	11	183	±	7	3.3	±	0.3	0.99777
15AlCl3:10BuA	172	±	16	611	±	14	179	±	9	3.6	±	0.4	0.99795
17AlCl3:10BuA	208	±	12	368	±	7	71	±	2	1.8	±	0.1	0.99764
10AlCl3:10PrA	183	±	8	529	±	6	157	±	3	2.9	±	0.2	0.99951
11AlCl3:10PrA	163	±	21	633	±	16	214	±	10	3.9	±	0.6	0.99740
13AlCl3:10PrA	163	±	24	639	±	26	252	±	6	3.9	±	0.5	0.99634
15AlCl3:10PrA	167	±	8	619	±	7	209	±	4	3.7	±	0.2	0.99964
17AlCl3:10PrA	163	±	10	645	±	8	202	±	5	3.9	±	0.3	0.99955

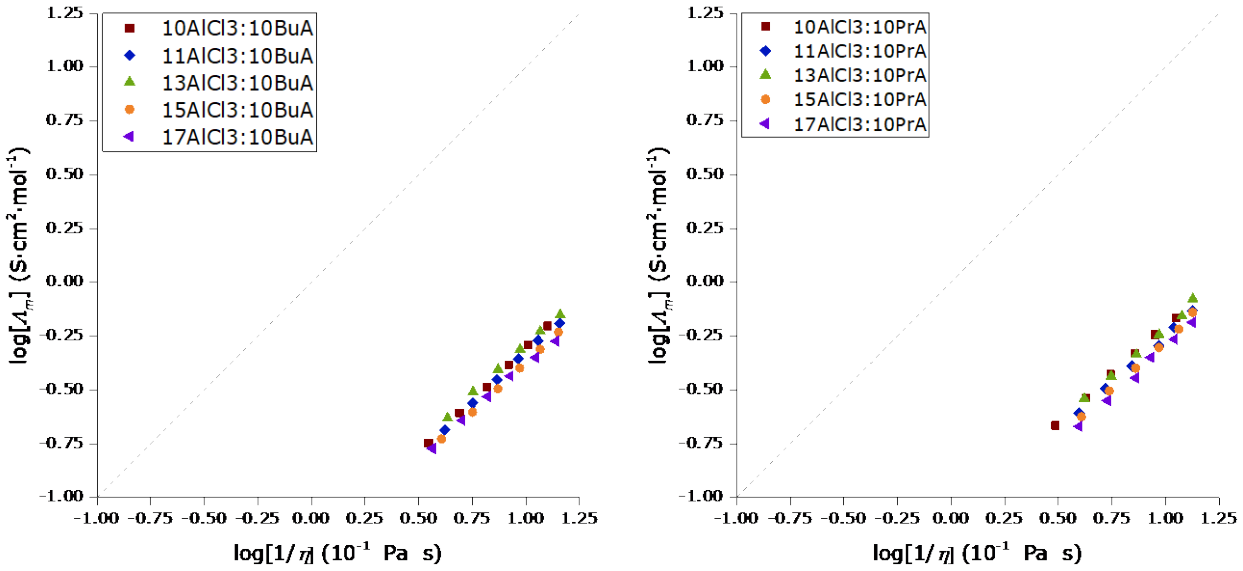

Figure 4. Walden Product plots for variable molar ratios of $AlCl_3$:BA (left) and $AlCl_3$:PA (right). The dashed line is the ideal line for a 0.01 M aqueous KCl solution.

Table 2. Walden Product fitted parameters, including the correlation coefficient of determination (COD-R^2).

Sample	W	StdErr	Adj R^2	Vertical Distance from y=x
10AlCl3:10AcA	1.01	0.02	0.99798	-1.115
11AlCl3:10AcA	0.93	0.01	0.99939	-1.182
13AlCl3:10AcA	0.99	0.01	0.99955	-1.160
15AlCl3:10AcA	1.01	0.02	0.99887	-1.200
--	--	--	--	--
10AlCl3:10BuA	0.98	0.01	0.99970	-1.300
11AlCl3:10BuA	0.93	0.01	0.99872	-1.321
13AlCl3:10BuA	0.91	0.01	0.99892	-1.282
15AlCl3:10BuA	0.92	0.01	0.99959	-1.364
17AlCl3:10BuA	0.87	0.02	0.99645	-1.366
--	--	--	--	--
10AlCl3:10PrA	0.89	0.01	0.99939	-1.180
11AlCl3:10PrA	0.89	0.02	0.99654	-1.235
13AlCl3:10PrA	0.89	0.03	0.99394	-1.198
15AlCl3:10PrA	0.92	0.02	0.99773	-1.259
17AlCl3:10PrA	0.92	0.02	0.99667	-1.290

2. NMR Spectra: Variable temperature ^{1}H and ^{27}Al spectra for all DES electrolytes were collected over the temperature range of 293-363K. The reference used for both nuclei was 1M $AlCl_3$ in H_2O, and the reference frequency was set to 0 ppm for both nuclei. It should be noted that typically tetramethylsilane (TMS) is the ^{1}H reference and that the hydrogen atoms in water resonates at about 4.7 ppm downfield (higher frequency) of TMS. In spite of the reference choice, the characterization of the proton groups and their respective shielding afforded by the neighboring electrons remains precise. The ^{1}H spectra for $AlCl_3$:AA showed two asymmetric peaks corresponding to the CH_3 and NH_2 groups, with peak areas ratio of 3:2 for all concentrations and temperatures. The ^{1}H spectra for the $AlCl_3$:PA samples showed the NH_2, CH_2, and CH_3 groups in the ratio of 2:2:3 as expected, representing the number of hydrogen atoms of each group. Spectra for the 1.1:1 molar ratio of both $AlCl_3$:AA (left) and $AlCl_3$:PA (right) are shown in Figure 5. The ^{1}H spectra for the $AlCl_3$:BA samples showed the NH_2, α-CH_2, β-CH_2 and CH_3 groups also in the expected 2:2:2:3 integral ratio.

In general, the dissociation of $AlCl_3$ in the amides means the resulting cations and anions can be solvated by solvent molecules forming their respective solvation spheres, with the remaining solvent molecules forming the bulk solvent. On the NMR timescale, these various environments would be spectroscopically discernable if the exchange rate between the hydrogen atoms in the various environments were slow. The fact that the peaks observed are mostly single component albeit asymmetric, suggests fast exchange between the various environments. Because

of this, the chemical shift values observed are averages of all the groups in the various environment.

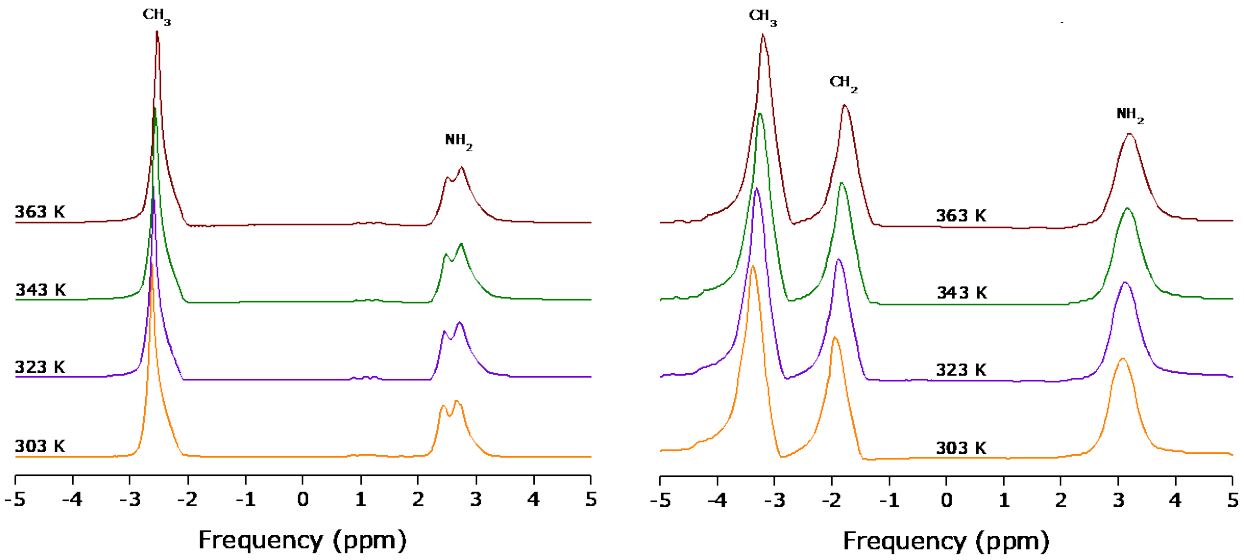

Figure 5. ^{1}H variable temperature spectra for 1.1:1 (left) $AlCl_3$:AA and 1.1:1 (right) $AlCl_3$:PA.

^{1}H Spectra: For all three amides, the ^{1}H chemical shifts for all groups fell in the range expected for typical organic solvents [47]. As previously stated, the measurements were repeated four times and the results presented are the average of all. Additionally, the spectra and chemical shifts were reversible with decreasing temperature. For all three amides and all molar ratios, the CH_3 group's chemical shift occurred at lower frequencies compared to those of the NH_2 group. This was also the case for their powdered form as well as their 1M solutions with D_2O as the solvent. This means the CH_3 hydrogen atoms are more diamagnetically shielded compared to the amides', which could be due to the interaction between the carbonyl group's carbons and the amide's nitrogen atom. Although both proton groups are attached to the carbonyl which is known to cause deshielding in its neighbors, the amide's nitrogen atom is known to donate electron density to directly bonded carbonyl carbons. The result of this is the formation of pi-bonds which are restrictive and allow limited motion about the C-N bond. Additionally, because of the nitrogen atom's donation, the electron density is delocalized over the pi-bond and is therefore less available for shielding of the amides' hydrogen atoms or for localized Coulombic interactions. A representative depiction of this is shown in Figure 6 for $AlCl_3$:PA electrolytes.

For both $AlCl_3$:AA and $AlCl_3$:BA electrolytes, the NH_2 peak became split for concentrations above the 1:1 molar ratio. This may be the result of intramolecular coupling between the amide's hydrogen atoms and neighboring hydrogens, since intermolecular dipole-dipole ones would be less effective. Interestingly, this splitting was not observed in the $AlCl_3$:PA electrolytes for any concentration or temperature. Additionally, a small triplet was observed between 0 – 2 ppm for all amides and molar ratios, and decreased in intensity with increasing molar ratio. This signal may be due to impurities, or bulk amide molecules which are expected to decrease as more $AlCl_3$ is added to the system. For each amide and molar ratio, the chemical shift of the triplet was insensitive to temperature changes, suggesting hydrogen bonding was not a significant contributor to the interactions present in this environment.

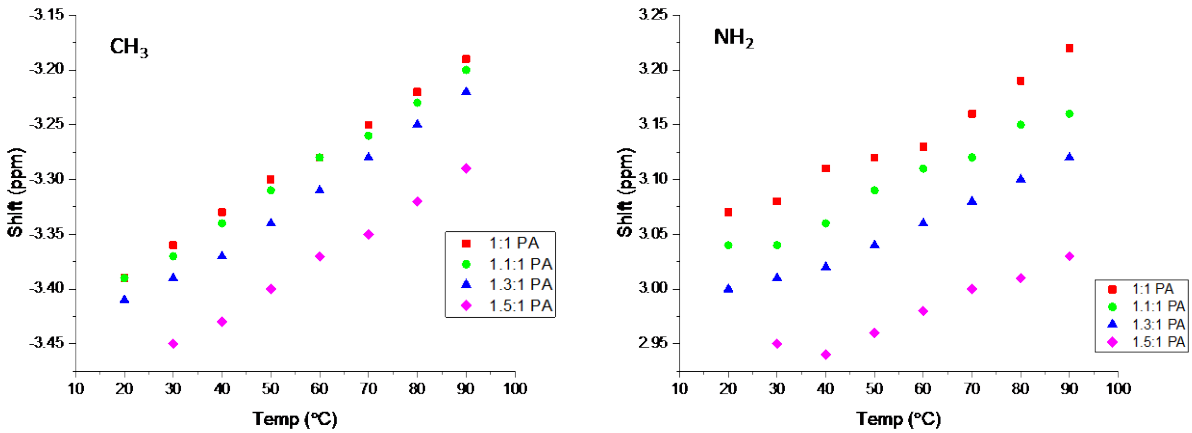

Figure 6. ^{1}H variable temperature chemical shift data for the 1:1- 1.5:1 molar ratio $AlCl_3$:PA electrolytes.

For all DES electrolytes the ^{1}H chemical shift was only modestly affected by both temperature and increasing molar ratio. The general behavior was a decrease in shielding with increasing temperature. This is expected since increasing temperature will increase the bond lengths, thereby decreasing the surrounding electron densities. The addition of the $AlCl_3$ to the amides caused a significant increase in shielding for the proton groups. For example, the chemical shifts for the CH_3 and NH_2 groups in the powered acetamide occurred at -1.56 ppm and 4.08 ppm respectively. However, with the addition of the $AlCl_3$ these peaks occurred at -2.57 ppm and ~2.71 ppm respectively. Additionally, further increase in $AlCl_3$ content continued to increase the shielding of the proton groups in all amides.

According to Hu et. al. [16] the equilibria processes for $AlCl_3$ and amide can occur through three pathways, with the formation of anionic and cationic structures such as $AlCl_4^-$, $Al_2Cl_7^-$, and $[AlCl_2(amide)_n]^+$ where n = 1 and 2. Examples of the three possible equilibria are presented in equations 9-11 [16]:

$$2[AlCl_3L_n] \leftrightarrow [AlCl_2L_n]^+ + [AlCl_4]^- + nL \quad [9]$$

$$2[AlCl_3L_n] + Al_2Cl_6 \leftrightarrow 2[AlCl_2L_n]^+ + 2[AlCl_4]^- \quad [10]$$

$$2[AlCl_4]^- + Al_2Cl_6 \leftrightarrow 2[Al_2Cl_7]^- \quad [11]$$

where L represents the amide. At low molar ratios, reaction 9 is favored. With increasing $AlCl_3$ concentration, the equilibrium shifts to reaction 10, and finally at higher molar ratios reaction 11 becomes the norm. Proton chemical shifts are dependent on several factors including the local conformational symmetry. The increased shielding observed with increasing molar ratio suggests an increase in the various electron densities, which could support a move in the equilibrium of equation 9 to one in which there is a greater concentration of anionic species as supported by equations 10 and 11. Additionally, since an increase in $AlCl_3$ concentration will cause a decrease in the available free volume, proton groups are expected to be within closer proximity with each other. Simultaneously, there will also be shorter separation distances between the various ionic species. One direct result of this reduced separation is greater inter- and intra- molecular dipole-dipole interactions, which could enhance the local electron densities ergo shielding. There could

also be restrictions in the conformational *cis-trans* dynamics of the amide molecules such that they adopt the conformation that enhances local electron densities. Generally, for terminally bonded protons the chemical shift for the *trans* molecule conformation is greater (less shielded) compared to the *cis* conformation [47]. The increasing shielding with increasing $AlCl_3$ concentration could therefore cause an increase in the *cis* conformations at higher concentrations. There were no noticeable differences in the linewidth of any proton group with increasing molar ratio. This suggests that although the increasing $AlCl_3$ concentration could be reducing the available free volume, the change is not substantial enough to restrict the proton groups rotational motions and that these motions are faster than the spectral (*us*) timescale [22, 47-48].

^{27}Al Spectra: Generally, aluminum in solution is very reactive and interacts strongly with the donor atoms [49]. Because of this, the species present in a system will depend on the solvent, the dissolved aluminum compound, and the nature of any other component present [47]. The chemical shift range of aluminum consists of mainly three regions [47]. These are: alkylaluminum compounds at frequencies greater than 150 ppm, tetrahedrally coordinated aluminum between 140 and 40 ppm, and from hexagonally to octahedrally coordinated aluminum species between 40 and -46 ppm. While there may be exceptions, these regions are generally the norm. Because of this, the chemical shift can be used as an indicator for the coordination number and the local symmetry.

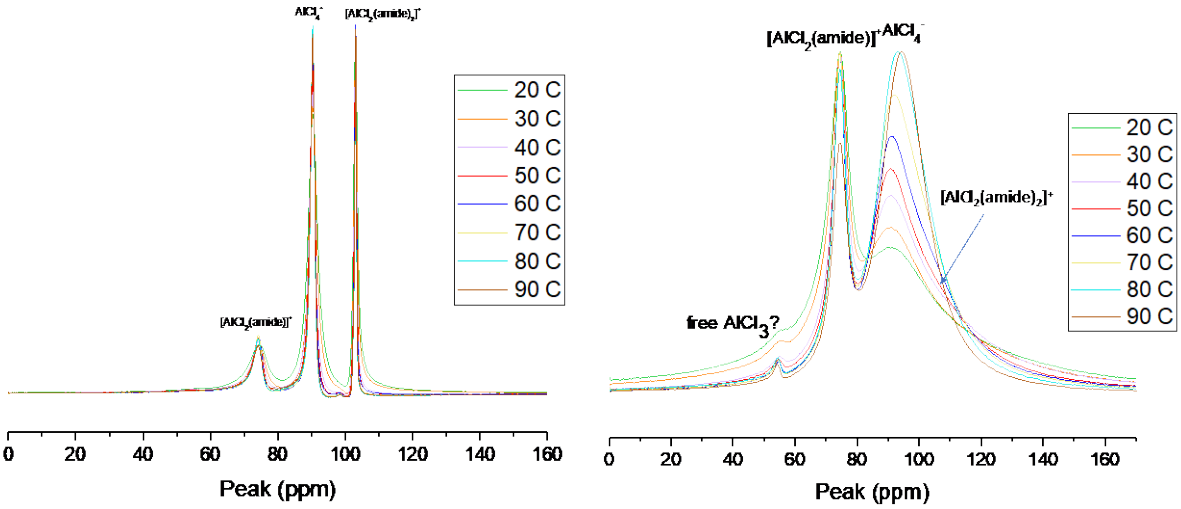

Figure 7. ^{27}Al variable temperature spectra for 1:1 (left) and 1.3:1 (right) $AlCl_3$:PA.

For all 1:1 molar ratio DES electrolytes three peaks at about 101, 88 and 74 ppm were observed, indicating the presence of tetrahedrally coordinated aluminum species. A representative plot is shown in Figure 7 (left) for the 1:1 molar ratio $AlCl_3$:PA electrolyte with our chosen assignments as: $[AlCl_2(amide)_2]^+$, $AlCl_4^-$, and $[AlCl_2(amide)]^+$ species respectively [12,18]. These assignments are the same as those of Abood et.al. [12], who performed both fast atom bombardment mass spectroscopy (FAB-MS) and ^{27}Al NMR spectra to assess the aluminum speciation for the 1:1 molar ratio $AlCl_3$:AA DES electrolyte. Their assignment of the $AlCl_4^-$ peak was based on its integration to almost the sum of the other two peaks. Additionally, they found the integration peak ratio of $[AlCl_2(amide)_2]^+$ to $[AlCl_2(amide)]^+$ to be 1.6:1, which is similar to our result of 1.5. Abbott et.al. also observed similar results for the 1:1 molar ratio $AlCl_3$:Urea DES

[18]. As stated previously, these peaks also bear different species assignment including: δ = ~102 ppm, 88 ppm, and 72 ppm as $AlCl_4^-$, $[AlCl_3(amide)]$, and $[AlCl_2(amide)_2]^+$ respectively [17]. A fourth peak has also been observed for higher $AlCl_3$ concentrations at ~ 54 ppm and has been assigned as neutral $[AlCl_3(amide)_2]$ [17].

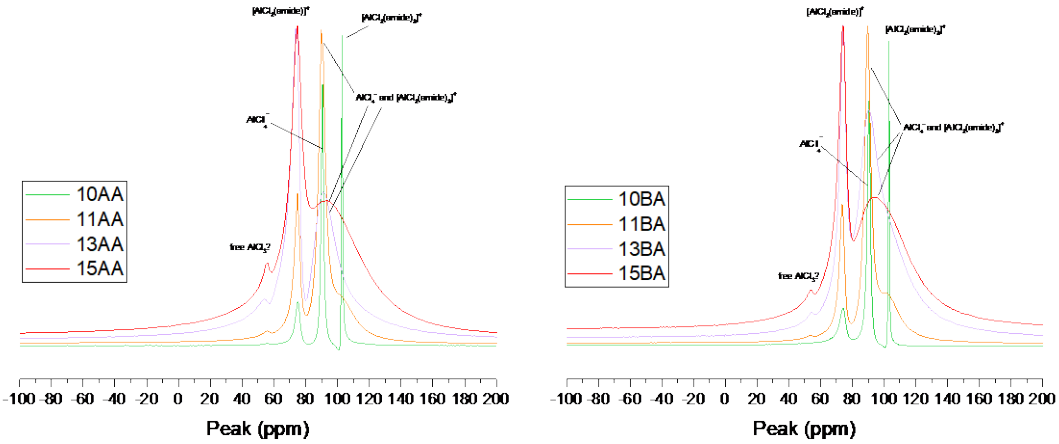

Figure 8. ^{27}Al NMR spectra for the 1:1-1.5-1 molar ratios of $AlCl_3$:AA (left) and $AlCl_3$:BA (right) at 323K.

The increasing temperature caused no noteworthy changes in the chemical shifts for the 1:1 molar ratio DES electrolytes. An analysis of the linewidth however revealed the presence of more species that the assigned ones. This was demonstrated for the 1:1 molar ratio $AlCl_3$:AA electrolyte, which required the use of six peaks to improve the residual of the Mestrenova deconvolution procedure as shown in Figure S5 of the Supporting Information. Since these peaks do not have separate resonances, we surmised that they resulted from the presence of multiple species (including $Al_2Cl_7^-$ and $Al_3Cl_{10}^-$) that are experiencing fast chemical exchange with each other on the NMR timescale. Although the equilibria condition expressed in Equation 9 [16] does not account for any additional species, the linewidths of the 1:1 molar ratio electrolyte suggests otherwise. Due to the fast exchange, as well as the lack of population information and identification of the various species, it was not possible to determine if the exchange was due to conversion of species (i.e. $AlCl_4^-$ to $Al_2Cl_7^-$, etc.), or convergence of their respective chemical shifts due to changes in their local environments mediated by increasing molar ratios.

For molar ratios greater than 1:1, the assigned $AlCl_4^-$ and $[AlCl_2(amide)_2]^+$ peaks merged, and only modest changes (~1 ppm) were observed with increasing temperatures. Similar to the 1:1 molar ratio electrolyte, a more noteworthy observation was the effect of $AlCl_3$ concentration on the linewidth, which showed significant line broadening resulting from increasing molar ratio for all species and all amides. Examples of this are shown in Figure 7 (**right**) for $AlCl_3$:PA and in Figure 8 for the $AlCl_3$:AA (**left**) and $AlCl_3$:BA (**right**) electrolytes, and selective deconvolution plots are shown in Figure S6 of the Supporting Information. Due to the merging of the assigned $AlCl_4^-$ and $[AlCl_2(amide)_2]^+$ peaks the line broadening observed is likely due to a combination of fast chemical exchange, where the aluminum spins are able to sample the magnetic fields created by both the $AlCl_4^-$ and $[AlCl_2(amide)_2]^+$ species, and the increasing electric field gradient the aluminum spins experience due to the greater $AlCl_3$ concentration. In chemical exchange between two-sites of equal spin populations [47], the two distinct peaks observed during the slow exchange

process becomes a merged, broadened flat-topped single peak at intermediate exchange rates. The frequency of this broadened flat-topped peak is the magnitude of the difference between the two chemical shifts ($\delta\nu = \nu_A - \nu_B$), and the exchange rate k is ~$2.2\delta\nu$. As shown in Figure 9 (left), the spin populations for the $AlCl_4^-$ and $[AlCl_2(amide)_2]^+$ species are not equal. However, it is clear that while increasing molar ratio increases the $AlCl_4^-$ species at the expense of the $[AlCl_2(amide)_2]^+$ species, that this is a dynamic process and not a complete conversion as evident by the merged peak's chemical shift. At this point it must also be noted that for molar ratios greater than 1:1, the peak assigned to $AlCl_4^-$ is also itself an average of the dialuminum heptachloride ($Al_2Cl_7^-$) and the chemically similar $AlCl_4^-$ species. Although resolution of the $Al_2Cl_7^-$ species was not directly observed possibly due to the fast exchange between it and the chemically similar $AlCl_4^-$, the broadening of the assigned $AlCl_4^-$ peak with increasing molar ratios should therefore be viewed as the average of at least the $Al_2Cl_7^-$, $AlCl_4^-$ and $[AlCl_2(amide)_2]^+$ species. This is further supported by MestreNova deconvolution of the 1.5:1 $AlCl_3$:PA (at 323K, **left**) and the 1.3:1 $AlCl_3$:BA (at 333K, **right**) electrolytes. As shown in Figure S6, the two peaks (in blue) used to fit the shaded region are centered at the respective chemical shift for the $[AlCl_2(amide)_2]^+$ and $AlCl_4^-$ species. However, there is a residual (in orange) that is more obvious for the butyramide electrolyte, which could account for the presence of additional species including $Al_2Cl_7^-$. As stated previously, the concentration of the $[AlCl_2(amide)_2]^+$ species decreases with increasing temperature. Therefore, it is likely the linewidth used in the deconvolution is overly generous and should be reduced, thereby enhancing the spectral presence of the $Al_2Cl_7^-$ species.

Integral area percentages were determined using the normalization method of the peak areas for all amides and concentrations with well resolved peaks. Examples of these results are shown in Figure 9 for the 1:1 and 1.3:1 molar ratio $AlCl_3$:AA electrolytes. Additional plots for the 1:1 and 1.1:1 molar ratios of $AlCl_3$:BA and $AlCl_3$:PA are shown in Figures S7 and S8 respectively of the Supporting information.

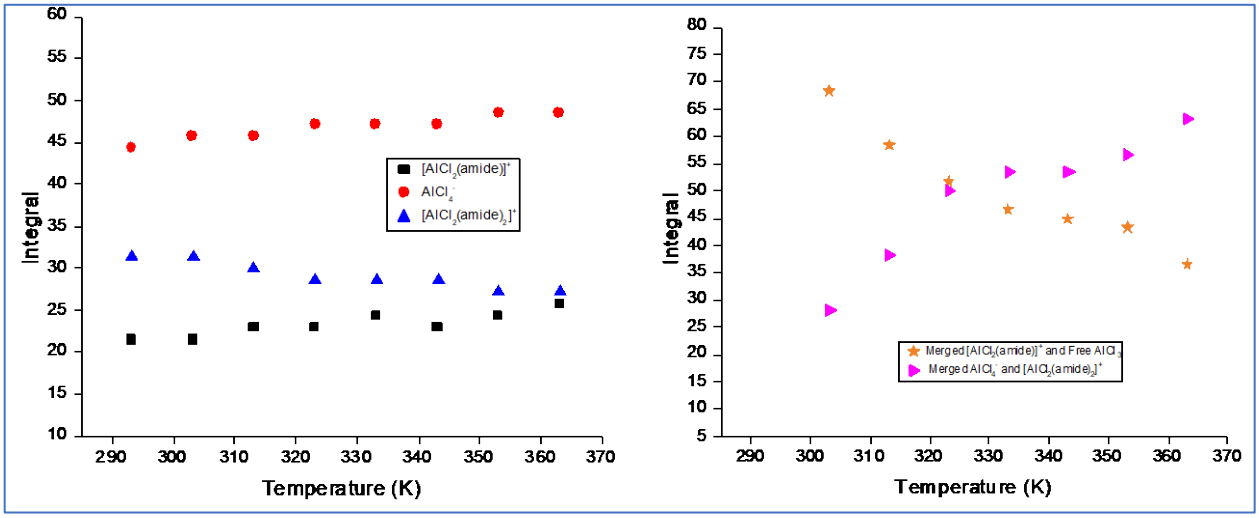

Figure 9. Integral percentages of the aluminum species for the 1:1 (**left**) and 1.3:1 (**right**) molar ratios $AlCl_3$:AA electrolytes.

For all three amides and at the 1:1 molar ratio, the integral area of the composite $AlCl_4^-$ peak was largest and as stated previously. This was followed by the $[AlCl_2(amide)_2]^+$ peak and

finally by the $[AlCl_2(amide)]^+$ peak at lower temperatures. However, whereas the $AlCl_4^-$ and $[AlCl_2(amide)]^+$ peaks integral areas increased with increasing temperature, that for the $[AlCl_2(amide)_2]^+$ decreased, providing another deciding factor in our chosen species assignment. This behavior was observed for all 1:1 molar ratio $AlCl_3$:amide DES electrolytes (see Figure 9(**left**)) and is explained as follows. As stated previously, Hu et.al. [16] gives the possible equilibrium pathways shown in equations 9-11. At the 1:1 molar ratio reaction 9 applies. If cationic structures for both n = 1 and 2 are present, increasing temperatures will increase the Al-C bond lengths, thereby reducing the integral of the n = 2 species. This reduction would manifest as an increase in the other species. Support for this argument is provided by Chu et.al. [14] who performed DFT calculations on the 1.3:1 $AlCl_3$:AA electrolyte in order to determine the equilibrium pathways capable of producing Al_2S_3 during the discharge process of the Al-S battery. They assumed the possibility of various species (cationic, anionic, and neutral), and determined two viable pathways which are expressed in equations 12-13:

$$Al_2Cl_7^- \rightarrow 7/4AlCl_4^- + 1/4Al^{3+} \quad [12]$$

$$½[AlCl_2(amide)_2]^+ \rightarrow 1/4AlCl_4^- + 1/4Al^{3+} + amide \quad [13]$$

Whereas both pathways were found to be exothermically energetically favorable, the binding energy of the second was found to be higher by 0.28 eV, thereby making it less favorable. With increasing temperatures however, the expectation is that this pathway will become more favorable, thereby increasing the $AlCl_4^-$ species and others at its expense. Additionally, since the interactions between the amide molecules and the aluminum species are expected to be dominated not only by electrostatic interactions but also by hydrogen bonding as is often the case with fragile liquids, increasing temperatures will definitely cause a reduction in the hydrogen bonding network's strength and breadth, thereby making it more favorable for smaller solvated species at higher temperatures.

While the integral percentage for the $AlCl_4^-$ peak increased from ~45-50 for both the acetamide and propionamide electrolytes over the temperature range, that for butyramide had the greatest increase, spanning a range of ~45-55. This could be an indication of a weaker hydrogen bonding network by the butyramide compared to the acetamide and propionamide. Compared to both propionamide and acetamide, butyramide is most bulky and because of this, its interacting with the various ionic species could be less effective. A factor that would have supported butyramide providing the weakest hydrogen bonding is its dielectric constant, which unfortunately at the time of writing was unavailable. In fact, only values for acetamide were. However, values for their N-methyl analogues were available and at 30°C, the dielectric constants are 178.9, 164.3 and 124.7 respectively for N-methylacetamide [42-43], N-methylpropionamide [49-50] and N-methylbutyramide [51]. Since the strength of the hydrogen bonding network as well as the local electrostatic interactions are modulated by the dielectric screening of the amide molecules, the butyramide analogue having the lowest dielectric constant would support it also providing a weaker hydrogen bonding network.

For molar ratios greater than 1:1, a fourth peak at about 54 ppm became more pronounced for all the $AlCl_3$:amides and examples of this are shown in Figure 8. This peak also appeared in the 1:1 molar ratio of the $AlCl_3$:amides but was very small in intensity and linewidth. As previously stated, this peak has also been observed by other researchers and was assigned as neutral $[AlCl_3(amide)_2]$ [17].

Spin lattice relaxation time - T_1:

Spin-lattice relaxation for spin I = ½ nuclei is caused by dynamical fluctuations in local magnetic fields that oftentimes result mainly from dipolar interactions, chemical shift anisotropy (CSA), scalar couplings, and spin rotations. CSA results from the changing magnetic fields that are experienced when molecules tumble in fluids. However, the magnitude of CSA for hydrogen is very small. Additionally, while the rotation of methyl and methylene groups can affect spin-lattice relaxation, the largest contributor for hydrogen relaxation is generally the dipole-dipole interactions. For quadrupole nuclei (I > ½) there is an additional and generally more efficient mechanism – the quadrupole interaction – which results from the nucleus' inherent quadrupole moment that allows it to interact with electric field gradients external to the nucleus. Regardless of the type of spin, several factors can influence the spin-lattice relaxation time T_1. These include group or species type, location, size, symmetry and temperature.

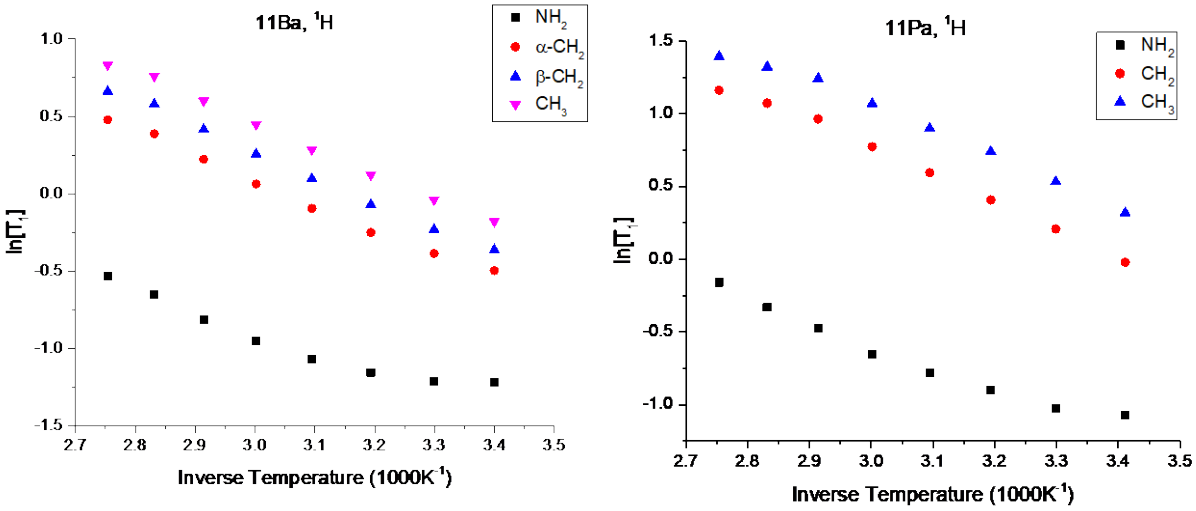

Figure 10. Variable temperature ^1H T_1 Arrhenius plots for 1.1:1 molar ratio $AlCl_3$:BA (left) and $AlCl_3$:PA (right).

The general trend for all $AlCl_3$:amide was an increase in the ^1H T_1 with increasing temperature for all groups (CH_3, CH_2, NH_2) and concentrations. A representation of this is shown in Figure 10 for 1.1:1 molar ratio $AlCl_3$:BA and $AlCl_3$:PA electrolytes. Additional plots for the $AlCl_3$:AA electrolytes are shown in Figures S9 and S10 of the Supporting Information. According to the BPP theory [22] the total spin-lattice relaxation rate for homonuclear dipole-dipole interaction is given by the relationship in Eq. 3 and is the sum of the intramolecular and intermolecular relaxation rates ($1/T_{1,intra} + 1/T_{1,inter}$). For fast molecular motions, the T_1 increases and becomes frequency independent. This is called motional narrowing. The increasing nature of the ^1H T_1 means we are in the extreme or motional narrowing regime.

Depending on their location, CH_2, CH_3 and NH_2 groups can rotate about their principal axes. In the case of the CH_3 and NH_2 groups, for all amides studied they occupy terminal positions which means they should have more rotational freedom. Generally, rotational motions make the dipole-dipole relaxation mechanism less efficient at the observed Larmor frequency. This is because of the averaging of the local magnetic fields that are responsible for relaxation, which can result in longer T_1 values. For all amides, the terminal CH_3 and NH_2 groups generally had the

longest and shortest T_1 values respectively for all concentrations and all temperatures. This suggests the rotational motion of the methyl group about its principal C_{3V} axis is faster compared to that of the amide and CH_2 groups about their respective C_{2V} axes. Generally, rotational or intramolecular dynamics about molecular axes tend to be faster compared with intermolecular dipolar ones. This is because intermolecular dynamics fluctuate much more slowly due to the time dependent long-range Brownian motions of whole molecules. In addition to this, the r^{-6} dependence of the homonuclear dipole-dipole interaction almost guarantees that the dominant participants are intramolecular hydrogen atoms, ergo rotational dynamics.

An additional factor that caused the amide group to have the shortest T_1 value is the fact that it is directly bonded to a carbonyl group (C=O). As previously stated, the nitrogen atom donates electron density to create a pi-bond with the carbonyl carbon. Pi-bonds have restrictive rotational motion, therefore the amide group is expected to rotate much more slowly compared to the terminal methyl group, thereby resulting in shorter T_1 values. The β-CH_2 group of butyramide had longer T_1 compared to the α-CH_2. This may also be due to the proximity of the α-CH_2 to the carbonyl group which will causes reduced mobility ergo shorter T_1.

A comparison of the CH_3 group T_1 values show that with the exception of the 1:1 molar ratio, the propionamide DESs having the longest T_1 values at all temperatures and the butyramides having the shortest. A similar comparison of the NH_2 group T_1 values show the general order for the DES electrolytes being: AA > PA ≥ BA for all temperatures, which coincides with the expected dielectric screening of the amides. These results suggest that (1) the NH_2 group's rotational motion increases with increasing dielectric screening, and (2) the CH_3 group requires an environment that provides a balance between the flexibility associated with shorter alkyl chains, and the electrostatic screening afforded by greater dielectric constants. An additional feature observed in the NH_2 T_1 data was the broad minimum for all molar ratios and amides. An example of this is shown in the Arrhenius plots for the 1.1:1 molar ratios of the $AlCl_3$:BA and $AlCl_3$:PA DESs (Figure 10). The BPP theory [22] states that at the T_1 minimum $\omega_0\tau_c \cong 1$ and the relaxation mechanism is most efficient. However, when a broad minimum is observed it generally indicates multiple relaxation mechanisms are in effect. As previously stated, the dominant relaxation mechanism for protons is the homonuclear dipole-dipole interaction. However, there can be contributions from normally lesser contributing mechanisms which - due to the reduced rotational motion of the NH_2 group – increases in magnitude. The minimum also became broader with increasing molar ratio, further supporting the increasing contributions of other relaxation mechanisms.

The ^{27}Al T_1 were also determined and representative plots are shown in Figure 11 for the 1.1:1 molar ratio $AlCl_3$:BA (left) and $AlCl_3$:PA (right) electrolytes. Additional plots are given in Figure S11 and S12 of the Supporting Information. Similar to the proton T_1 data, all aluminum T_1 data were single exponentials. As stated previously, aluminum is a quadrupole nucleus and its relaxation mechanisms are dominated by quadrupole interactions [22, 52]. In the case of single exponential T_1 data, two conditions produce this result. The first is the extreme narrowing condition where $\omega_0\tau_c << 1$ for isotropic small-step rotational diffusion, the quadrupole spin-lattice ($1/T_{1Q}$) and spin-spin ($1/T_{2Q}$) relaxation rates are given by [22, 52]:

$$\frac{1}{T_{1Q}} = \frac{1}{T_{2Q}} = \frac{3\pi^2}{10}\frac{(2I+3)}{I^2(2I-1)}\left(1+\frac{\eta^3}{3}\right)\left(\frac{e^2qQ}{h}\right)^2\tau_C \qquad [14]$$

where τ_c represents the motional correlation time. As shown and was generally observed, the aluminum T_1 increases with increasing temperature for all species, indicating the motion is in the

extreme narrowing regime. If the motion is not isotropic but still in the extreme narrowing regime, the relaxation rates can still be equal in the event the surrounding electric field gradient is axially symmetric ($\eta_Q = 0$). Regardless, the quadrupole relaxations can result from both intra- and inter-molecular electric field gradients whereby the magnitude and orientation of the principal axis system varies with time. This is especially relevant in ionic liquid systems where the motions of the various charge distributions cause fluctuations at the site of the quadrupole nucleus.

As shown in Figure 7(left) for the 1:1 molar ratio $AlCl_3$:PA electrolyte, the lowest concentration ^{27}Al spectra showed three main peaks, located at about 101, 88 and 74 ppm for the $[AlCl_2(amide)_2]^+$, $AlCl_4^-$, and $[AlCl_2(amide)]^+$ species respectively [12,18]. Similar to the proton data, the aluminum T_1 showed dependencies on species type and salt concentration. With increasing $AlCl_3$ concentration the concentration of $Al_2Cl_7^-$ (and possibly $Al_3Cl_{10}^-$) is expected to increase according to Hu et. al. [16] and expressed in Equations 9-11. However, as stated previously, due to its chemical similarity to $AlCl_4^-$ and the fast exchange between them on the NMR timescale in the temperature range studied, no separation between their signals was observed. In addition to this, the assigned $AlCl_2(amide)_2^+$ and averaged $AlCl_4^-$ peaks merged with increasing molar ratio, and a single T_1 was determined. This T_1 is therefore the average of several species including - $AlCl_2(amide)_2^+$, $AlCl_4^-$, $Al_2Cl_7^-$, and $Al_3Cl_{10}^-$.

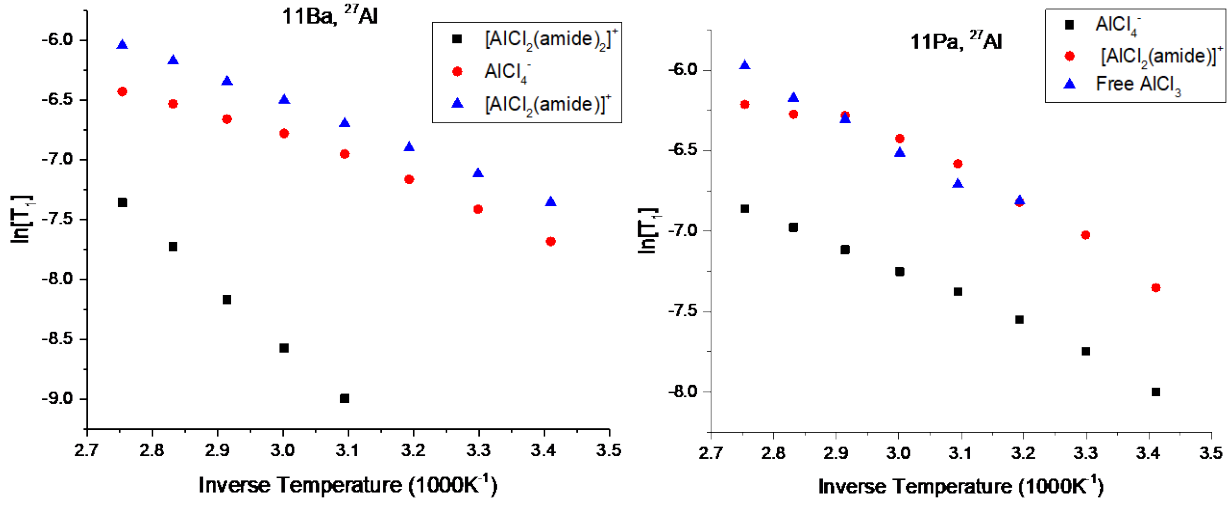

Figure 11. Variable temperature ^{27}Al T_1 Arrhenius plots for 1.1:1 molar ratio $AlCl_3$:BA (left) and $AlCl_3$:PA (right).

Unlike the proton T_1, that for all separable aluminum peaks decreased with increasing molar ratio for all amide types. With increasing $AlCl_3$ concentration, the available free volume will decrease. This in turn will reduce the aluminum species rotational small-step rotational diffusion motions, and increases the effect of the surrounding electric field gradients and the strength of the quadrupolar relaxation mechanism. Since the quadrupole relaxation mechanism is generally very dominant compared to the other relaxation mechanisms for spin $I > ½$ nuclei [22, 45], the increasing and efficient quadrupole relaxation mechanism will result in decreasing T_1 with increasing molar ratios, as was observed.

For the 1:1 molar ratio electrolyte, the peak at ~101 ppm assigned to the $AlCl_2(amide)_2^+$ species had the longest T_1, while that at ~74 ppm assigned to the $AlCl_2(amide)^+$ was the shortest.

This pattern was reversed for the 1.1:1 molar ratio $AlCl_3$:BA electrolyte, and likely indicates a conversion point where $AlCl_2(amide)_2^+$ species are being decreased. For the 1.1:1 molar ratio acetamide and propionamide DES electrolytes the $AlCl_2(amide)_2^+$ is indistinguishable, and the composite $AlCl_4^-$ peak had the shortest T_1 over the entire temperature range while the $AlCl_2(amide)^+$ had the longest. This pattern continued for the higher molar ratios of all three amides at all temperatures. Since both the mobility and the surrounding electric field gradients can affect the T_1 for quadrupole nuclei, we compared the masses of the species. For both propionamide and butyramide the order of the aluminum species masses is as follows: $AlCl_3 < AlCl_4^- < AlCl_2(amide)^+ < AlCl_2(amide)_2^+$. For acetamide, the order is: $AlCl_3 < AlCl_2(amide)^+ < AlCl_4^- < AlCl_2(amide)_2^+$. For all three amides, the $AlCl_2(amide)_2^+$ species has the largest mass and would therefore have the most restriction to both translational and whole molecule rotational motions. Similarly, the $AlCl_3$ has the smallest. In the motional narrowing regime, a stronger electric field gradient will result in shorter quadrupole spin lattice relaxation times. Based upon this, these results suggest that when it is distinguishable and in equilibrium the $AlCl_2(amide)_2^+$ species experiences the smallest electric field gradient, while the composite $AlCl_4^-$ species experiences the largest. For higher concentrations (>1.1:1 molar ratio), the peak at ~54 ppm assigned to the free $AlCl_3$ became more prominent and the determined T_1 values were longer than those for the composite $AlCl_4^-$ species for all temperatures, molar ratios and amide types, which could be due to a combination of its smaller mass and possibly smaller electric field gradient.

Further comparison of the effect of $AlCl_3$ concentration on the T_1 values for the various species revealed a temperature and concentration dependent plateauing in the T_1 of the $AlCl_2(amide)^+$ species for molar ratios greater than 1:1. This was first observed for the 1.3:1 molar ratio of both the acetamide and butyramide electrolytes as shown in Figures S13-14 of the Supporting Information, where the onset temperature was 343K. The T_1 for the 1.3:1 propionamide electrolyte however continued to increase albeit at a slower rate. The trend observed for all three amides persisted for the 1.5:1 molar ratio but the onset temperature for the acetamide electrolyte was lowered to 323K. In 1.7:1 molar ratio all three amides showed plateaus, with the onset temperature for both propionamide and butyramide being 343K, and that for acetamide remaining at 323K. Unlike the $AlCl_2(amide)^+$ species, that for $AlCl_4^-$ was an increase in T_1 with increasing temperature for all molar ratios.

Activation energies were determined for the proton and aluminum groups and are presented in Tables 3 and 4 respectively. For the NH_2 group, only the linear portion of the Arrhenius data were used in the respective activation energy determination. Values for the proton groups ranged from ~9 – 15.5 kJ/mol, while those for the aluminum species ranged from ~2 – 40 kJ/mol. The proton values are similar to values obtained for common imidazolium-based cations such as $EMIM^+$ [26] and $BMIM^+$ [27], both of which are known to have conformational flexibility in their alkyl chains. The large difference between the activation energy values tells of the difficulty in rotational mobility the aluminum species experience compared to the protons. Whereas the activation energies for the free $AlCl_3$ and $AlCl_2(amide)^+$ species decrease with increasing molar ratio, that for the composite $AlCl_4^-$ species generally increased. As previously stated, the composite $AlCl_4^-$ species experiences greater electric field gradients. Because of this, the local electrostatic interactions will also be stronger which can severely restrict the species' rotational and translational mobilities. The result of these would be a need for greater activation energies.

Table 3. Activation energies in kJ/mol for ^1H spin-lattice relaxation times in the $AlCl_3$:amide (AcA – acetamide, PrA – propionamide, and BuA – butyramide) analogues.

1H T1 Activation Energy* (kJ·mol^{-1})					
Sample	**NH_2**	**CH_2**	**α-CH_2**	**β-CH_2**	**CH_3**
10AlCl3:10AcA	10.9				9.9
11AlCl3:10AcA	11.2				11.3
13AlCl3:10AcA	9.5				10.0
15AlCl3:10AcA	12.0				13.5
17AlCl3:10AcA	13.2				13.2
10AlCl3:10BuA	13.5		13.0	13.6	14.1
11AlCl3:10BuA	12.1		13.1	13.7	13.5
13AlCl3:10BuA	10.9		13.7	14.3	13.9
15AlCl3:10BuA	11.6		14.4	14.8	14.8
17AlCl3:10BuA	8.7		14.1	14.4	13.3
10AlCl3:10PrA	14.1	12.6			13.1
11AlCl3:10PrA	14.1	15.3			14.0
13AlCl3:10PrA	9.2	15.1			14.3
15AlCl3:10PrA	13.5	15.4			14.2
17AlCl3:10PrA	10.0	15.2			14.1

* All values have a standard error of ±0.1 kJ·mol^{-1}

Table 4. Activation energies in kJ/mol for ^{27}Al spin-lattice relaxation times in the $AlCl_3$:amide (AcA – acetamide, PrA – propionamide, and BuA – butyramide) analogues.

27Al T1 Activation Energy* (kJ·mol^{-1})				
Sample	**$[AlCl_2(amide)_2]^+$**	**$[AlCl_4]^-$**	**$[AlCl_2(amide)]^+$**	**Free $AlCl_3$**
10AlCl3:10AcA	26.8	20.9	19.0	
11AlCl3:10AcA		12.7	17.2	19.6
13AlCl3:10AcA		17.8	8.8	
15AlCl3:10AcA		27.4	0.8	
17AlCl3:10AcA		25.7	-4.5	
10AlCl3:10BuA	15.8	16.7	22.6	
11AlCl3:10BuA	40.2	15.8	16.7	
13AlCl3:10BuA		16.5	11.9	24.4
15AlCl3:10BuA		22.0	7.3	9.3
17AlCl3:10BuA		25.6	4.2	1.9
10AlCl3:10PrA	21.7	16.5	17.8	
11AlCl3:10PrA		14.1	16.3	16.2
13AlCl3:10PrA		19.5	8.6	10.2
15AlCl3:10PrA		31.5	5.8	9.8
17AlCl3:10PrA		27.3	1.9	11.7

* All values have a standard error of ±0.1 kJ·mol^{-1}

Summary:

In this study, the variable temperature NMR spin-lattice relaxation times and spectra, and ionic conductivity measurements were determined for varying molar ratios of $AlCl_3$:amide (acetamide, propionamide and butyramide) deep eutectic solvents. Results were generally dependent on amide type, $AlCl_3$ concentration and temperature, and suggests an interdependent and complex ionic mobility system. Firstly, the aluminum species populations were mostly dependent on $AlCl_3$ concentration and temperature, and less so on amide type. For example, for the 1:1 molar ratio electrolytes, ^{27}Al spectra showed three peaks at about 101, 88 and 74 ppm

which were assigned as the $AlCl_2(amide)_2^+$, $AlCl_4^-$, and $AlCl_2(amide)^+$ species respectively. For all the electrolytes, the $AlCl_2(amide)_2^+$ species had the longest T_1 and the $AlCl_2(amide)^+$ species had the shortest. However, whereas the populations of the $AlCl_4^-$, and $AlCl_2(amide)^+$ species increased with increasing molar ratio, that for the $AlCl_2(amide)_2^+$ species decreased, suggesting a thermally activating cleaving of the amide molecules resulting in a possible conversion to other aluminum species whose chemical shifts corresponds to both the $AlCl_4^-$ and $AlCl_2(amide)^+$ species. This type of cleaving could also be indicative of the presence of hydrogen bonding between the amide molecules as they are known to break (reduce) with increasing temperature. Unfortunately, the $AlCl_2(amide)_2^+$ peak was not separable for concentrations above the 1:1 molar ratio except for the 1.1:1 $AlCl_3$:BA electrolyte, where the determined T_1 were significantly reduced compared to those for both the $AlCl_4^-$ and $AlCl_2(amide)^+$ species. These results also suggest the $AlCl_2(amide)_2^+$ species plays a less significant role in the ionic transport with increasing $AlCl_3$ concentration, especially for shorter alkyl chain amides.

Secondly, whereas the ^{27}Al T_1 decreased with increasing $AlCl_3$ concentration, the opposite was observed for the proton groups, regardless of amide type. Additionally, the T_1 for the terminal proton groups showed amide type dependences, where the NH_2 groups not only had shorter T_1 compared to the CH_3 groups, but were more susceptible to local electrostatic interactions which was emphasized by their broad T_1 minima for all molar ratios and amides. With regards to the ^{27}Al T_1, results show the composite $AlCl_4^-$ species having the shortest T_1 values regardless of amide type, temperature and molar ratio. This was attributed to it having the largest electric field gradient of all the aluminum species. Unlike the T_1 for the $AlCl_4^-$ species which increased with increasing temperature, that for $AlCl_2(amide)^+$ species showed a temperature, concentration and amide dependent plateau for molar ratios greater than 1.1:1. These differences show a contrast in the respective local environments of the two species. Whereas the $AlCl_4^-$ species dynamics is dominated by the local electric field gradients, it appears that for the $AlCl_2(amide)^+$ species is also dependent on the flexibility of the amides' alkyl chains, the motion of which causes some reduction in the strength of the electric field gradients the $AlCl_2(amide)^+$ species experience.

Thirdly, the short-range aluminum species dynamics showed clear influence on the bulk ion transport. As discussed, the ionic conductivity for both the propionamide and butyramide DES electrolytes displayed a prominent maximum at the 1.3:1 molar ratio, while the acetamide DESs showed a broad plateau starting at the 1.1:1 molar ratio at lower temperatures giving way to a more pronounced maximum at the 1.3:1 molar ratio at higher temperatures. Since the population of the composite $AlCl_4^-$ peak increased while that for the $[AlCl_2(amide)]^+$ peak decreased with increasing molar ratio for all amides, the ionic conductivity maximum is mostly due to the mobility of the $AlCl_4^-$, $Al_2Cl_7^-$, and $Al_3Cl_{10}^-$ species. This is supported by the increasing T_1 for the $AlCl_4^-$ species and the plateauing of that for the $AlCl_2(amide)^+$ species with increasing temperature.

Of the three amides, propionamide seems the most suitable for high $AlCl_3$ concentration applications that will allow the formation and efficient transport of the $AlCl_2(amide)^+$ and $Al_2Cl_7^-$ species, both of which have been surmised as deposition routes for aluminum metal. It offers a balance between the competing effects of dielectric screening, and bulkiness and packing afforded by its alkyl chain. Additionally, its alkyl chain was the most mobile which allowed faster *cis-trans* conversions.

With regards to their application as electrolytes in AIBs, the deep eutectic solvent (DES) must exhibit fast (translational, conformational, and rotational) ionic and molecular dynamics. Both the VFT and Walden Product analyses were instrumental in revealing fast conformational motions. The presence of these local conformational motions and fluctuations assists in ionic

diffusion, not only through reduced molecular packing ergo viscosity, but through the shuttling of ionic species like the aluminum that rely on the Vehicle transport mechanism. When coupled with the NMR spin-lattice relaxation time and spectral measurements, the picture that emerges is one of a complex interplay of Coulombic dominated interactions, mixed with coordinated ionic mobilities and ion associations, being mediated by the dielectric shielding of the amides. Although preliminary, these results support the possibility of tuning the DES mixtures for desired applications.

Acknowledgement: This work was supported by the National Science Foundation, Solid State and Materials Chemistry Program, Division of Materials Research, EAGER award # 1841398. The BC College Now program provided support for the Midwood High School students who participated during the 2019 summer program. Special thanks to Dr. Philip Stallworth of Hunter College (CUNY) for his technical help at crucial times during this project.

References:

1. M. Armand, J.-M. Tarascon, Building better batteries, Nature 451 (2008) 652-657.
2. H. Chen, M. Armand, M. Courty, M. Jiang, C.P. Grey, F. Dolhem, J.M. Tarascon, P. Poizot, Lithium salt of tetrahydroxybenzoquinone: toward the development of a sustainable Li-ion battery, J. Am. Chem. Soc. 131 (2009) 8984-8988.
3. B. Dunn, H. Kamath, J.M. Tarascon, Electrical energy storage for the grid: a battery of choices, Science 334 (2011) 928-935.
4. K. Hayamizu, S. Tsuzuki, S. Seki, K. Fujii, M. Suenaga, Y. Umebayashi, Studies on the translational and rotational motions of ionic liquids composed of N-methyl-N-propyl-pyrrolidinium (P_{13}) cation and bis(trifluoromethanesulfonyl)amide and bis(fluorosulfonyl)amide anions and their binary systems including lithium salts, J. Chem. Phys., 133, (2010) 194505.
5. K. Ueno, J.-W. Park, A. Yamazaki, T. Mandai, N. Tachikawa, K. Dokko, and M. Watanabe, Anionic Effects on Solvate Ionic Liquid Electrolytes in Rechargeable Lithium−Sulfur Batteries, J. Phys. Chem. C., 117 (2013) 20509.
6. B. Geĺinas, M. Natali, T. Bibienne, Q. P. Li, M. Dolle, and D. Rochefort, Electrochemical and transport properties of ions in mixtures of electroactive ionic liquid and propylene carbonate with a lithium salt for lithium-ion batteries, J. Phys. Chem. C., 120 (2016) 5315.
7. H.-T. Kim, J. Kang, J. Mun, S. M. Oh, T. Yim, and Y. G. Kim, Pyrrolinium-based Ionic Liquid as a Flame Retardant for Binary Electrolytes of Lithium Ion Batteries, ACS Sustainable Chem. Eng., 4 (2016) 497.
8. M. L. Phung Le, F. Alloin, P. Strobel, J.-C. Lepretre, C. P. del Valle, and P. Judeinstein Structure-Properties Relationships of Lithium Electrolytes Based on Ionic Liquid, J. Phys. Chem. B, 114 (2010) 894.
9. F. Castiglione, E. Ragg, A. Mele, G.B. Appetecchi, M. Montanino, and S. Passerini, Molecular Environment and Enhanced Diffusivity of Li Ions in Lithium-Salt-Doped Ionic Liquid Electrolytes, J. Phys. Chem. Lett., 2 (2011) 153.
10. M.L. Douche, J.J. Rameau, R. Durand, F. Novel-Cattin, Electrochemical behaviour of aluminium in concentrated NaOH solutions, Corros. Sci. 41, (1999), 805.

11. M. Zhang, V. Kamavarum, R.G. Reddy. New electrolytes for aluminum production: Ionic liquids. The Journal of The Minerals. 55, (2003), 54-57.
12. H.M.A. Abood, A.P. Abbott, A. D. Ballantyne, and K.S. Ryder, Do all ionic liquids need organic cations? Characterization of $[AlCl_2{*}nAmide]^+AlCl_4^-$ and comparison with imidazolium based systems, Chem. Commun., 47, (2011) 3523.
13. Y. Zhao, T.J. VanderNoot, Electrodeposition of Aluminium from Nonaqueous Organic Electrolytic Systems and Room Temperature Molten Salts, Electrochim. Acta, 42 (1997), 3−13.
14. W. Chu, X. Zhang, J. Wang, S. Zhao, S. Liu, H. Yu, Energy Storage Materials, (2019), https://doi.org/10.1016/j.ensm.2019.01.025.
15. B. Guchhait, S. Das, S. Daschakraborty, and R. Biswas, Interaction and dynamics of (alkylamide + electrolyte) deep eutectics: Dependence on alkyl chain-length, temperature, and anion identity, J. Chem. Phys., 140, (2014), 104514.
16. P. Hu, R. Zhang, X. Meng, H. Liu, C. Xu, and Z. Liu, Structural and spectroscopic characterizations of amide-AlCl3-based ionic liquid analogues, Inorganic Chemistry, 55, (2016) 2374.
17. M. Angell, C.-J. Pan, Y. Rong, C. Yuan, M.-C. Lin, B.-J. Hwang, and H. Dai, High Coulombic efficiency aluminum-ion battery using an $AlCl_3$-urea ionic liquid analog electrolyte, PNAS, 114 (2017) 834.
18. A. P. Abbott, R. C. Harris, Y.-T. Hsieh, K. S. Ryder and I.-W. Sun, Aluminium electrodeposition under ambient conditions, Phys. Chem. Chem. Phys., 16, (2014) 14675.
19. F. Coleman, G. Srinivasan, M. Swadźba-Kwasńy, Liquid Coordination Complexes Formed by the Heterolytic Cleavage of Metal Halides, Angew. Chem., Int. Ed. 52, (2013) 12582−12586.
20. J. Estager, P. Nockemann, K. R. Seddon, M. SwadzbaKwasny, S. Tyrrell, Validation of Speciation Techniques: A Study of Chlorozincate(II) Ionic Liquids, Inorg. Chem., 50, (2011) 5258.
21. C. Liu, W. Chen, Z. Wu, B. Gao, X. Hu, Z. Shi, Z. Wang, Density, viscosity and electrical conductivity of $AlCl_3$-amide ionic liquid analogues, J. Molecular Liquids, 247 (2017) 57.
22. A. Abragam, Principles of Nuclear Magnetism, Oxford University Press, 1961.
23. S.H. Chung, S. Bajue, S.G. Greenbaum, Mass transport of phosphoric acid in water: A ^1H and ^{31}P pulsed gradient spin-echo nuclear magnetic resonance study, J. Chem. Phys., 112, (2000), 8515-8521.
24. J.R.P. Jayakody, S.H. Chung, L. Durantino, H. Zhang, L. Xiao, B.C. Benicewicz, S.G. Greenbaum, NMR Studies of Mass Transport in High-Acid-Content Fuel Cell Membranes Based on Phosphoric Acid and Polybenzimidazole, J. Electrochem. Soc., 154, (2007), B242-B246.
25. S. Suarez, S. Greenbaum, J. Fontanella, T. Zawodzinski, A Fundamental Study of the Transport Properties of Aqueous Superacid Solutions, J. Physical Chemistry B, 114, (2010), 8941-8947.
26. S. Suarez, A. Rua, D. Cuffari, K. Pilar, J. Hatcher, S. Ramati, J. Wishart, Do TFSA Anions Slither? Pressure Exposes the Role of TFSA Conformational Exchange in Self-Diffusion. Journal of Physical Chemistry B, 119, (2015), 14756-14765.
27. K. Pilar, A. Rua, S.N. Suarez, C. Mallia, S. Lai, J. Jayakody, Jasmine L. Hatcher, James F. Wishart, Steve Greenbaum, Investigation of Dynamics in BMIM-TFSA ionic liquid

through variable temperature and pressure NMR relaxometry and diffusometry. Journal of the Electrochemical Society,164, (2017), H5150-5159.

28. J.L. Gray, G.E. Maciel, Aluminum-27 Nuclear Magnetic Resonance study of the room temperature melt aluminum trichloride butylpyridinium chloride, J. Am. Chem. Soc., 103, (1981), 7147-7151.
29. S. Takahashi, M.L. Saboungi, R.J. Klingler, M.J. Chen, J.W. Rathke, Dynamics of room temperature melts: nuclear magnetic resonance measurements of dialkylimidazolium haolauminates, J. Chem. Soc., Faraday Trans., 89, (1993), 3591-3595.
30. J.S. Wilkes, J.S. Frye, G.F. Reynolds, Aluminum-27 and carbon-13 NMR studies of aluminum chloride dialkylimidazolium chloride molten salts, Inorg. Chem., 22, (1983), 3870-3872.
31. J.S. Seo, K.W. Kim, H.G. Cho, Spectrochim. Acta, Part A 2003, 59, 477−486.
32. M. Dalibart, J. Derouault, P. Granger, S. Chapelle, Inorg. Chem. 1982, 21, 1040−1046.
33. C.A. Angell, Formation of glasses from liquids and biopolymers, Science, New Series, 267 (1995) 1924-1935.
34. T.G. Fox, P.J. Flory, Second order transition temperatures and related properties of polystyrene. 1. influence of molecular weight, J. Applied Phys., 21 (1950) 581.
35. J.T. Bendler, J.J. Fontanella, M. F. Shlesinger, J. Bartos, O. Sausa, J. Kristiak, Free-volume dynamics in glasses and supercooled liquids, Phys. Rev. E., 71 (2005) 031508.
36. G. Dlubek, Y. Yu, R. Krause-Rehberg, W. Beichel, S. Bulut, N. Pogodina, I. Krossing, Ch. Friedrich, Free volume in imidazolium triflimide [C_3MIM][NTf_2] ionic liquid from positron lifetime:amorphous, crystalline, and liguid states, J. Chem. Phys., 133 (2010) 124502.
37. M. S. Shannon, J.M. Tedstone, S. P.O. Danielsen, M. S. Hindman, A.C. Irvin, J.E. Bara, Free volume as the basis of gas solubility and selectivity in imidazolium-based ionic liquids, Ind. Eng. Chem. Res., 51 (2012) 5565-5576.
38. W. Beichel, Y. Yu, G. Dlubek, R. Krause-Rehberg, J. Pionteck, D. Pfefferkorn, S. Bulut, D. Bejan, C. Friedrich, I. Krossing, Free volume in ionic liquids: a connection of experimentally accessible observables from PALS and PVT experiments with the molecular structure from XRD data, Phys. Chem. Chem. Phys., 15 (2013) 8821.
39. N. J. Brooks, F. Castiglione, C. M. Doherty, A. Dolan, A. J. Hill, P. A. Hunt, R. P. Mathews, M. Mauri, A. Mele, R. Simonutti, I. J. Villar-Garcia, C. C. Weber, T. Welton, Linking the structures, free volumes, and properties of ionic liquid mixtures, Chem. Sci., 8 (2017) 6359-6374.
40. S. Ferrari, E. Quartarone, P. Mustarelli, A. Magistris, M. Fagnoni, S. Protti, C. Gerbaldi, A. Spinella, Lithium ion conducting PVdF-HFP composite gel electrolytes based on N-methoxyethyl-N-methylpyrrolidinium bis(trifluoromethanesulfonyl)-imide ionic liquid, J. Power Sources, 195 (2010) 559-566.
41. D.R. MacFarlane, M. Forsyth, E.I. Izgorodina, A.P. Abbott, G. Annat, K. Fraser, On the Concept of Ionicity in Ionic Liquids. Phys. Chem. Chem. Phys. 11 (2009) 4962−4967.
42. M. Yoshizawa, W. Xu, C.A. Angell, Ionic Liquids by Proton Transfer: Vapor Pressure, Conductivity, and the Relevance of pKa from Aqueous Solutions, J. Am. Chem. Soc. 125 (2003) 15411−15419.
43. J.P. Belieres, C.A. Angell, Protic Ionic Liquids: Preparation, Characterization, and Proton Free Energy Level Representation. J. Phys. Chem. B, 111 (2007) 4926−4937.

44. W. Xu, E. I. Cooper, C. A. Angell, Ionic Liquids: Ion Mobilities, Glass Temperatures, and Fragilities, J. Phys. Chem. B, 107 (2003) 6170.
45. M. Zhao, B. Wu, S. I. Lall-Ramnarine, J.D. Ramdihal Papacostas, E. D. Fernandez, R.A. Sumner, C.J. Margulis and E.W. Castner, Structural analysis of ionic liquids with symmetric and asymmetric fluorinated anions, J. Chem. Phys., 151 (2019) 074504.
46. G. A. Olah, G. K. Surya Prakash, G. Rasul, Reactions of superelectrophilic BH_2^+, BCl_2^+ and $AlCl_2^+$ with carbonyl compounds and alkenes, Arkivoc (2002) 7-18.
47. J. Mason, Ed., Multinuclear NMR, Plenum Press, New York, 1987.
48. M. H. Levitt, Spin Dynamics: Basics of Nuclear Magnetic Resonance, 2nd ed., John Wiley and Sons, England, 2008.
49. S. J. Bass, W. I. Nathan, R. M. Meighan, R. H. Cole, Dielectric properties of alkyl amides. II. Liquid dielectric constant and loss, J. Phys. Chem., 68 (1964), 509-515.
50. G.R. Leader, J.F. Gormley, The dielectric constant of N-Methylamides, JACS, 73, (1951) 5731-5733.
51. L.R. Dawson, R.H. Graves, P.G. Sears, Solvents having high dielectric constants. III. Solutions of sodium and potassium halides in N-methylpropionamide and in N-methylbutyramide from 30-60ºC, JACS, 79 (1957) 298-300.
52. J. Kowalewski, L. Mäler, Nuclear Spin Relaxation in Liquids: Theory, Experiments, and Applications, Taylor and Francis, New York, 2006.